






Hyperfine and nuclear quadrupole splitting of the NV^- ground state in $4H$ -SiC

F. F. Murzakhanov ¹, B. V. Yavkin ¹, G. V. Mamin ¹, S. B. Orlinskii,¹ H. J. von Bardeleben,² T. Biktagirov,³ U. Gerstmann ^{3,*} and V. A. Soltamov ^{1,†}

¹Kazan Federal University, Kazan 420008, Russia

²Sorbonne Université, Campus Pierre et Marie Curie, Institut des Nanosciences de Paris, 4, place Jussieu, 75005 Paris, France

³Lehrstuhl für Theoretische Materialphysik, Universität Paderborn, 33098 Paderborn, Germany



(Received 18 February 2021; accepted 8 June 2021; published 21 June 2021)

Optically addressable spin-triplet defects in silicon carbide, such as divacancies and negatively charged nitrogen vacancy (NV^-) allow to develop modern quantum technologies operating in the near-infrared range based on the well-developed semiconductor material. Here, by means of both high-frequency (94 GHz) pulsed electron paramagnetic resonance (EPR) and electron-nuclear double Resonance (ENDOR) techniques the ground state properties of the negatively charged NV^- defect in $4H$ -SiC were studied. We experimentally determined the ordering of the ground state spin sublevels and established the sign of the zero-field splitting to be positive as predicted by theory. Analysis of nuclear magnetic resonance transitions in ENDOR spectra allowed to determine the sign, symmetry, and absolute values of the hyperfine interaction of the NV^- defect electron spin with ^{14}N nuclear spin as $A_{\parallel} = -1.142$ MHz and $A_{\perp} = -1.184$ MHz. The absolute value of the nuclear quadrupole interaction constant reflecting an interaction between the ^{14}N nuclear electric quadrupole moment with the electric field gradient was determined to be $|C_q| = 2.44$ MHz. This large value is compatible with a threefold coordinated ^{14}N nucleus with uniaxial symmetry and proves conclusively the existence of a nearestneighbor $N_C V_{Si}$ pair in the material. For this NV^- defect, an ensemble (Hahn-echo) coherence time of $T_2 = 49 \mu s$ was measured, a value which is in the range previously reported for silicon vacancy spin ensembles and slightly longer than $T_2 = 40 \mu s$ measured here on the divacancy spin ensemble.

DOI: [10.1103/PhysRevB.103.245203](https://doi.org/10.1103/PhysRevB.103.245203)

I. INTRODUCTION

Spin-carrying defects in wide-band-gap crystalline materials are playing an important role in the development of modern quantum technologies [1–4]. The basic concept of their use is that the high spin state ($S \geq 1$) of the defect already splitted in zero magnetic field can be initialized, manipulated, and subsequently read out by optical or radio frequency means, providing an access to control the spin. This concept has been developed and successfully tested on a negatively charged nitrogen-vacancy (NV^-) defect in diamond. Thanks to the decades of intensive studies of the NV^- defect in diamond (see Ref. [5] and references therein), quantum networks and multi-qubit spin registers as well as quantum sensing and room temperature operated masers [1,6–9] have been developed, thus stimulated a search of such kind defects in solids more technologically friendly than diamond [10–12]. The most prominent results in this direction have been achieved on well-developed semiconductor material producing at the wafer-scale, such as silicon carbide (SiC) [2,3,13,14]. Indeed, a large variety of electron spin-triplet ($S = 1$) defects possessing optically addressable ground states with prominent coherence properties have been uncovered and identified in the most common SiC polytypes (3C, 4H, 6H) [12,15–18].

Namely, they are silicon-carbon divacancies and recently discovered the direct analog to the NV center in diamond, a negatively charged nitrogen vacancy center in form of a silicon vacancy (V_{Si}) with a nearest nitrogen atom substituting one of the carbon dangling bond atoms (N_C) [17,19].

In $4H$ -SiC, there are two nonequivalent crystallographic sites for Si and C, quasicubic (k) and hexagonal (h). This gives rise to four different configurations of the $N_C V_{Si}$ pair. Two configurations are axial relative the hexagonal c axis, $N_C(k)V_{Si}(k)$ and $N_C(h)V_{Si}(h)$ (further denoted as NV_{kk} and NV_{hh}), while two other configurations are basal, $N_C(k)V_{Si}(h)$ and $N_C(h)V_{Si}(k)$. The same notation logic applies to four divacancy configurations denoted as VV_{kk} , VV_{hh} , VV_{hk} , and VV_{kh} . In this work, we focus on defect pairs in axial configurations, namely on NV_{kk} , VV_{kk} , and VV_{hh} , as also illustrated in Fig. 1(a). All these defects possess sharp zero phonon lines in their optical recombination spectra close to the infrared telecom S and O bands; they are characterized by the moderate GHz value of the zero-field splitting (ZFS) in the ground state and can be controlled down to the single defect level [15,17,18,20–22]. These all together make triplet defects in SiC interesting candidates for quantum technologies. Since their first observation and identification by means of electron paramagnetic resonance (EPR) technique in the early 80s' [23], the divacancy centers have been intensively studied [21,24–26], so to date, their properties are quite well established. Unlike divacancies, NV^- centers in SiC have been observed relatively recently [16–18,20], so they still possess

*uwe.gerstmann@upb.de

†victrosoltamov@gmail.com

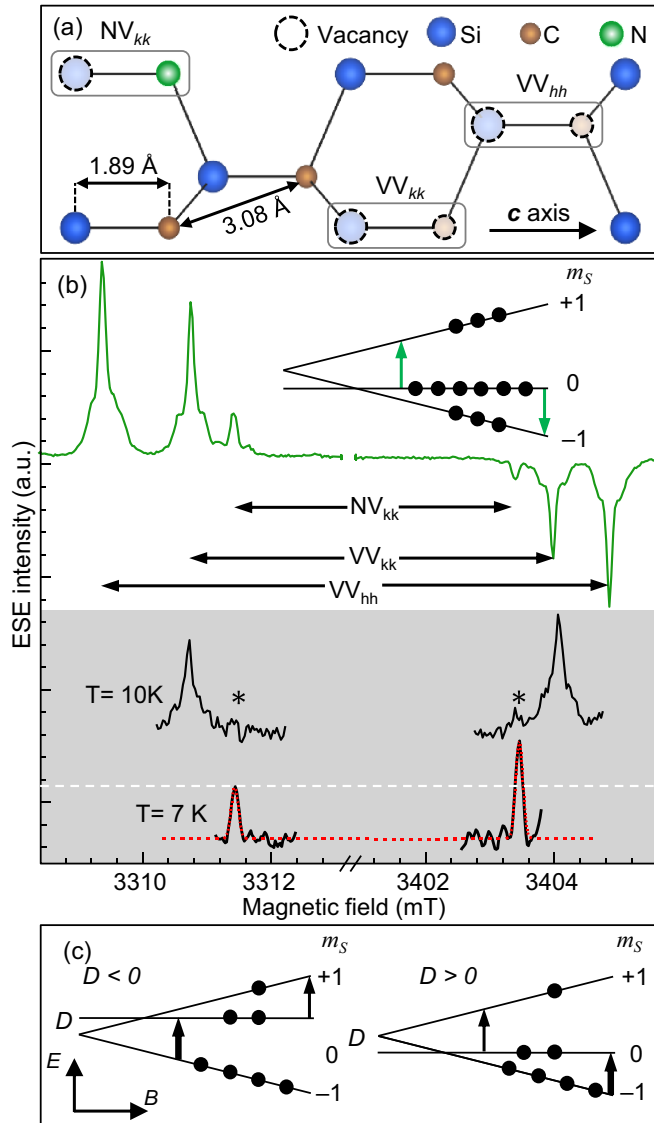


FIG. 1. (a) Models of the divacancies VV_{hh} , VV_{kk} together with NV_{kk} defect (highlighted by rectangles) in the 4H-SiC. Si and C vacancies are shown with dashed circles. 1.89 Å is the Si-C bond length along the *c* axis. 3.08 Å is the distance between basal C atoms. (b) (Top) Optically induced EPR spectrum of axial triplet centers in the 4H-SiC sample measured at temperature $T = 100$ K. Arrows show fine structure lines of the VV_{hh} , VV_{kk} , and NV_{kk} centers. The inset demonstrates optically induced predominant population of the $m_S = 0$ in the triplet ground state. (Bottom) EPR signals of VV_{kk} and NV_{kk} centers (marked with the asterisks) now measured at $T = 10$ and 7 K in the dark. Red-dashed line shows the simulated amplitude of the $T = 7$ K fine-structure lines. White-dashed line stress the difference in the EPR magnitudes. (c) Scheme of the Zeeman levels population due to Boltzmann distribution. Thick arrows show the $m_S = -1 \rightarrow m_S = 0$ transitions, depending on the sign of D value.

blind spots in their ground state properties, in particular with respect to the electron-nuclear interaction, that have to be filled for technological application.

In this paper, we focus on electron-nuclear interactions, in particular on the quadrupole interaction (QI) of the NV_{kk} center and on its coherence properties in comparison with the

axial $S = 1$ divacancies. Our experimental results are compared with theoretical predictions for the ENDOR-relevant spectroscopical data, namely, the hyperfine splitting and the quadrupole coupling constants. Our results further confirm the microscopic model of the NV centers as nearestneighbor $N_C V_{Si}$ pair defects in close analogy to the NV center in diamond. Alternative explanations like divacancy-distant N_C donor complexes have to be excluded: a large quadrupole splitting above 2 MHz is clearly indicative for a threefold coordinated ^{14}N nucleus.

II. EXPERIMENTAL METHOD

The sample used in this study with spatial dimensions 0.8 mm \times 0.4 mm \times 0.2 mm was cut from a commercially produced N-doped ($2 \times 10^{17} \text{ cm}^{-3}$) *n*-type 4H-SiC bulk crystal which has been irradiated at room temperature with 12-MeV protons to a total dose of $1 \times 10^{16} \text{ cm}^{-2}$ in order to produce the vacancy-type defects. The sample was then annealed at a temperature $T = 900$ °C, previously identified to be optimal for NV centers creation [17]. Electron spin echo-detected (ESE) EPR spectra were measured at W-band frequencies (≈ 94 GHz) on the Bruker Elexsys 680 spectrometer using standard Hahn-echo pulse sequence. NMR transitions between NV defects' nuclear spin sublevels were measured by means of electron-nuclear double resonance (ENDOR) technique using Mims pulse sequence. Spin-spin (T_2) relaxation curves were obtained using standard techniques to measure spin-echo decay.

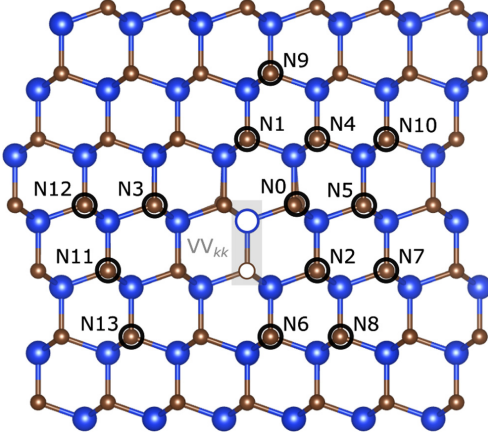
III. COMPUTATIONAL METHOD

In order to further analyze the experimental results, using density functional theory (DFT) we have calculated from *first principles* the relevant spectroscopical ENDOR data, hyperfine splittings and in particular the quadrupole splittings, for reasonable N-containing spin-triplet ($S = 1$) defect models. Besides the standard nearestneighbor NV pair we fully scan the ensemble of distant $(V_C V_{Si})_{kk}$ divacancy N_C donor complexes up to a distance of 7 Å (see also Table I and the figure therein). For the sake of completeness we also include the spin-triplet state of a minimum-distant $V_C V_{Si} N_C$ complex, which can be described as a combined divacancy-NV pair.

Following Ref. [17], we use supercells containing 432 atoms, standard norm-conserving pseudopotentials, a plane-wave basis with an energy cutoff of 50 Ryd and the spin-polarized PBE functional [27]. All defect structures have been fully relaxed using $2 \times 2 \times 2$ Monkhorst Pack (MP) *k*-point samplings. Whereas the calculated *g* tensors and ZFS parameters can be found elsewhere [16,17,28], we focus here on the hyperfine splittings and in particular on the electric field gradients (EFG) and quadrupole splittings [29]. All these parameters are calculated in scalar-relativistic approximation using the gauge-including projector augmented plane wave (GI-PAW) approach [30] as implemented in the QUANTUM ESPRESSO package [31,32].

More specifically, the hyperfine (hf) splittings are determined by the magnetization density $m(\vec{r})$ —the probability of the unpaired electron—in a small region around the nuclei [33,34]. The tensor of the quadrupole coupling, on the other

TABLE I. Hyperfine and quadrupole splittings calculated for the NV_{kk} and various divacancy- N_C^+ donor complexes. The positions of the N-donor atom with respect to VV_{kk} (shaded grey) are indicated in the sketch of the $4H$ -SiC lattice. Taking into account symmetry-related multiplicity the table covers 63 configurations. The data calculated for the second axial nearest-neighbor nitrogen vacancy center, NV_{hh} , are also presented.



model	Quadrupole C_q , MHz	(^{14}N) η	Hyperfine A_{xx}	(^{14}N) , A_{yy}	MHz A_{zz}	dE , eV
Expt.	-2.44	0.000	-1.142	-1.142	-1.184	
NV_{kk}	-2.313	0.000	-1.153	-1.153	-1.134	
NV_{hh}	-2.427	0.000	-1.079	-1.079	-1.115	
$VV_{kk} + N0$ (“ NV_{kk}^+ ”)	-1.957	0.058	4.369	4.161	9.291	0.000
$VV_{kk} + N1$	-0.021	0.000	-2.642	-2.642	-3.686	0.995
$VV_{kk} + N5$	-0.219	0.685	2.067	2.044	3.182	1.078
$VV_{kk} + N3$	0.146	0.574	-0.458	-0.605	-0.271	1.105
$VV_{kk} + N4$	-0.157	0.363	0.672	0.666	1.148	1.106
$VV_{kk} + N9$	0.115	0.065	0.087	0.072	0.183	1.159
$VV_{kk} + N12$	0.105	0.073	-0.065	-0.085	-0.002	1.210
$VV_{kk} + N10$	0.060	0.856	-0.021	-0.031	0.039	1.225
$VV_{kk} + N8$	0.097	0.272	-0.021	-0.025	0.047	1.351
$VV_{kk} + N11$	0.112	0.129	0.047	0.013	-0.012	1.352
$VV_{kk} + N13$	0.103	0.470	-0.046	-0.049	-0.012	1.341
$VV_{kk} + N7$	0.054	0.261	-0.023	-0.037	0.037	1.360
$VV_{kk} + N6$	0.172	0.655	-0.306	-0.310	-0.270	1.470
$VV_{kk} + N2$	0.407	0.309	0.787	0.733	1.051	1.477

hand, is related to the electrical field gradient (EFG) $V_{ij} = \frac{\partial^2 V}{\partial X_i \partial X_j}$ by $(C_q)_{ij} = eQ_N V_{ij}/h$, where $Q_N = 0.0204$ barn is the nuclear quadrupole moment of the ^{14}N nucleus and h the Planck constant.

IV. RESULTS AND DISCUSSION

First, we characterized the $4H$ -SiC sample by means of pulsed EPR measuring field-swept ESE spectrum under 532 nm optical excitation in the orientation of static magnetic field parallel to the hexagonal c axis ($\mathbf{B}||c$) of the crystal [Fig. 1(b)]. The sample demonstrates a large variety of defects responding by electron spin polarization on the optical excitation manifesting itself in phase reversal character of the EPR signals, corresponding to the emission/absorption of the microwave power, as schematically depicted in the inset in Fig. 1(b). They are spin-triplet divacancies with C_{3v}

symmetry, comprised the closest pair of the silicon and carbon vacancies occupying hexagonal (hh) and quasicubic (kk) sites in the $4H$ -SiC lattice [corresponding models of the centers are denoted as VV_{hh} and VV_{kk} in Fig. 1(a)]. Fine-structure transitions related to these defects are denoted in Fig. 1(b) according to the previously established values of their zero-filed splitting (ZFS) parameter D to be 1337 MHz for the VV_{hh} and 1306 MHz for VV_{kk} [12,25].

Additionally to the divacancies, another $S = 1$ defect with axially symmetric ZFS equal to 1288 MHz and g value of $g = 2.00194$ is observed. Previously, based on resolved ^{14}N hyperfine splitting this center was attributed to the negatively charged nitrogen-vacancy, comprising nitrogen atom substituting quasicubic (k) carbon atom (N_C) adjacent to the silicon vacancy in quasicubic position (V_{Si}) [16–18,20], i.e., the direct analogon to the NV^- center in diamond. There it was also shown, that the ZFS of NV_{kk} centers is temperature-dependent, varying with temperature between

1270–1290 MHz [16]. As revealed by theoretical studies, the single-particle level structure of axial NV centers in 4H-SiC is analogous to that of the diamond NV⁻ [35]. It features one a_1 orbital level and a degenerate e level deep within the band gap. The other a_1 level is located within the valence band. Both a_1 levels are fully occupied, whereas the degenerate e level is occupied by two electrons with parallel spins, giving rise to the triple ground state (3A_2). As in the divacancy case, under illumination, i.e., optical pumping of the Zeeman ground-state spin levels through an electron spin-dependent intersystem-crossing pathway the fine-structure EPR transitions undergo phase reversal.

Here we focus on the axial NV_{kk} center [cf. Fig. 1(a)], which is less affected by superposition with other centers. It thus allows a complete and robust analysis of the full spin Hamiltonian. We would like to note that NV_{hh} centers are characterized by a ZFS equal to $D = 1331$ MHz [18] very close to that of VV_{hh} centers. They are thus not directly seen in the EPR spectrum, since their fine-structure transitions interfere with those corresponding to the VV_{hh} centers.

We then established experimentally the energetic ordering of the triplet sublevels in the NV centers' ground state determined by the sign of the ZFS, as schematically shown in the inset in Fig. 1(c). To do so, the fine-structure EPR transitions without optical excitation and at low temperature ($T = 10$ and 7 K) are measured. As seen from the Fig. 1(b) especially for the spectrum measured at 7 K the magnitude of the high-field fine-structure component is larger than that of the low-field due to the thermal populations of the Zeeman levels governed by Boltzman factor $\exp(-h\nu/kT)$. At temperature $T = 7$ K and $\nu = 94$ GHz this factor is ≈ 0.525 conforms to the population probabilities of triplet spin sublevels to be 0.153, 0.291, and 0.555 for the $m_S = +1, 0,$ and -1 , respectively. Since the magnitude of the allowed magnetic dipole transitions is determined by the population differences of the corresponding spin sublevels, the magnitude of the $m_S = -1 \rightarrow m_S = 0$ transition is expected to be twice higher compared to the $m_S = 0 \rightarrow m_S = +1$. In the case of $D > 0$, the $m_S = -1 \rightarrow m_S = 0$ transition is expected in the high field, while in the case of $D < 0$ it is in the low field, in accordance with the scheme in Fig. 1(c). The observed magnitudes, together with their simulation using EASYSOFT software [36] reproduce this ratio nicely. Thereby, we can attribute the more intense high-field fine-structure component to the $m_S = -1 \rightarrow m_S = 0$ transition and deduce the positive sign of the D . This experimental observation is consistent with previously published theoretical results obtained by means of first principles DFT calculations [17]. After establishing the order of the Zeeman levels, we can identify that under optical excitation, the $m_S = 0$ sublevel is predominantly populated as schematically shown in the inset in Fig. 1(b), since the fine-structure line in the low magnetic field shows enhanced absorption, while the line in the high magnetic field demonstrates enhanced emission of the resonant microwaves.

We then use EPR spectrum measured without optical excitation (see Fig. S1 in Ref. [37]) to estimate the upper possible bound of the divacancies in our sample utilizing the NV_{kk} EPR signal as the reference. Indeed, in accordance with specification of the 4H-SiC crystal, the nitrogen concentration is $C(N) = 2 \times 10^{17}$ cm⁻³. Based on this, we can make a rough

estimate of NV concentration upper bound in our sample if considered that all nitrogen impurities are converted into the NV centers during annealing. Taking into account four possible configurations of NV centers, NV_{kk} concentration is $C(\text{NV}_{kk}) \leq 1/4 \times 2 \times 10^{17}$ cm⁻³ = 5×10^{16} cm⁻³. The integral intensity of EPR fine-structure lines for both VV_{kk} and VV_{hh} is three times larger than that of the NV_{kk}. Thereby the upper bound of the divacancies concentration in our sample is around 1.5×10^{17} cm⁻³ for each V_{kk} and VV_{hh} configuration.

A. Electron-nuclear interactions from ENDOR

The central part of our work deals with an as deep as possible analysis of the electron-nuclear interactions between optically polarised electron spins with the spin of the involved nitrogen nucleus. For this purpose, we induced nuclear magnetic resonance transitions associated with nitrogen. The transitions subsequently readout as changes in the ESE signal magnitude under NMR conditions by means of the Mims-type pulsed ENDOR technique [38]. The pulse sequence used in the experiment is the following. The first two $\pi/2$ mw pulses invert the electron spin population; the third $\pi/2$ pulse stimulates the ESE for signal detection. Between the second and the third mw pulses, a radio-frequency (RF) pulse is applied to invert the population of the nuclear spin sublevels for inducing NMR transitions.

In the following analysis and discussion of the EPR and ENDOR experiments, we consider an axially symmetric spin-Hamiltonian with nuclear quadrupole, hyperfine and fine-structure tensors all collinear having the c axis as the principal z axis:

$$H = g\mu_B \mathbf{B} \cdot \mathbf{S} + D(S_z^2 + \frac{1}{3}S(S+1)) - g_N \mu_N \mathbf{B} \cdot \mathbf{I} + A_{\parallel} S_z I_z + A_{\perp} (S_x I_x + S_y I_y) + P(I_z^2 + \frac{1}{3}I(I+1)), \quad (1)$$

where \mathbf{B} is the external static magnetic field, S is the electron spin operator with $S = 1$ the electron spin of the NV_{kk} defect. g and μ_B are the Landé g -factor and Bohr magneton, respectively, $g_N = +0.40376$ is the ¹⁴N nuclear g factor [39], μ_N is the nuclear magneton. I is the nuclear spin operator of the ¹⁴N nuclear spin ($I = 1$). The electron-nuclear hyperfine interaction parameters are denoted as A_{\parallel} , A_{\perp} and can be given in terms of the isotropic part represented by a and anisotropic part represented by b ($A_{\parallel} = a + 2b$, $A_{\perp} = a - b$). $P = \frac{3 \cdot eQ_N \cdot V_{zz}}{4I(2I-1)} = \frac{3}{4I(2I-1)} C_q$ is the axial nuclear quadrupole splitting parameter reflecting an interaction between the ¹⁴N nuclear electric quadrupole moment eQ_N with the largest principal component of the electric field gradient V_{zz} . The energy level scheme described by Eq. (1) is shown in Fig. 2(a) for the ($B \parallel c$) orientation.

The corresponding resonance conditions for nuclear spin flips in ENDOR experiments governed by the selection rules $\Delta m_S = 0$ and $\Delta m_I = 1$ are given by [40]

$$\nu = |-g_N \mu_N B + m_S(a + b(3 \cos^2 \theta - 1)) + m_q P(3 \cos^2 \theta - 1)|/h, \quad (2)$$

where $m_q = 1/2(m_I + m_I')$ is the average value of the two nuclear spin manifolds between which NMR transitions

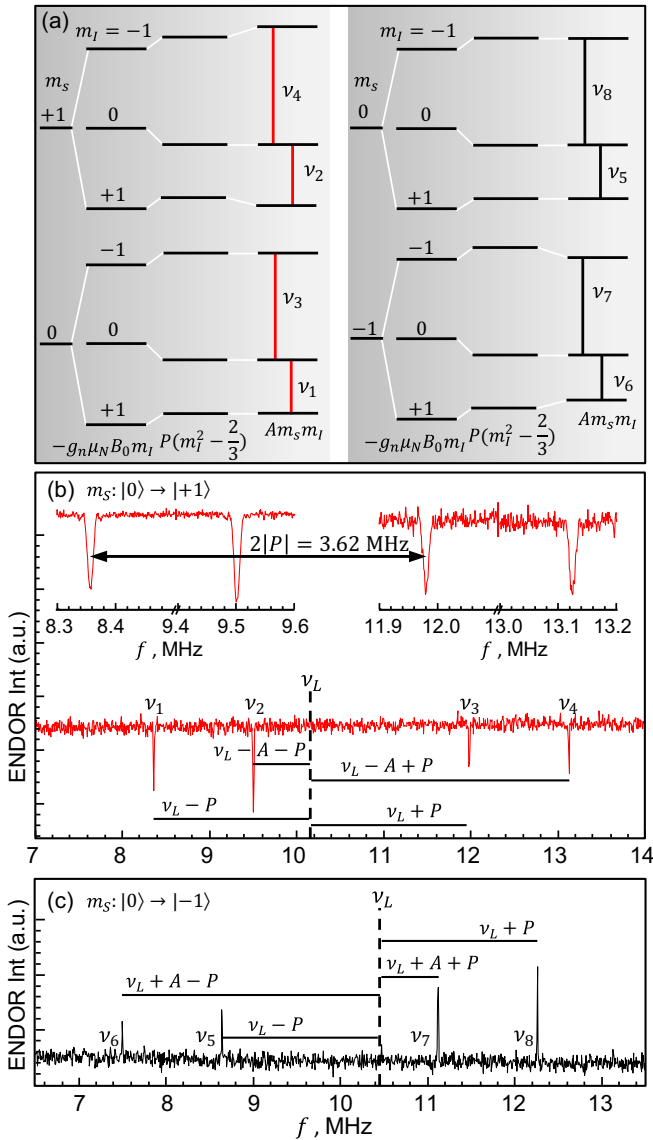


FIG. 2. (a) The scheme of the NV_{kk} ground state energy levels including nuclear Zeeman, hyperfine and quadrupole interactions with one ^{14}N nuclei. Expected ENDOR transitions for the fine-structure components $m_S = 0 \rightarrow +1$ (left panel) and $m_S = 0 \rightarrow -1$ (right panel) are shown with red and black bars, respectively. (b) ENDOR spectrum detected on the $m_S = 0 \rightarrow +1$ component, v_1 - v_4 transitions denoted in correspondence with the left panel of the scheme. Insets show the transitions in the enlarged scale, arrow indicates transitions due to the quadrupole splitting. (c) ENDOR spectrum detected on the $m_S = 0 \rightarrow -1$ ESE line, v_5 - v_8 transitions denoted as on the right panel of the scheme.

(denoted v_{1-8}) take place. For $I = 1$, there are two m_q values: $+1/2$ and $-1/2$. θ is the angle between static magnetic field and hexagonal c axis and $\nu_L = g_N \mu_N B/h$ is the nuclear Larmor frequency.

Figures 2(b) and 2(c) shows the ENDOR spectra measured on both $m_S = -1 \rightarrow 0$ and $m_S = 0 \rightarrow +1$ fine-structure EPR transitions. Each spectrum contains a set of all four frequencies, labeled following the diagram of Fig. 2(a). It should be noted, that for the $m_S = +1$ and $m_S = -1$ electron manifolds the ENDOR transitions are expected at $v_{2,4} = \nu_L - |A| \pm |P|$

and $v_{6,7} = \nu_L + |A| \pm |P|$, respectively. So one can establish the sign of the hyperfine constant A to be negative, since the highest frequency (v_4) is measured on the $m_S = 0 \rightarrow +1$ fine-structure EPR line. The absolute value of A is found as $|v_2 + v_4 - \nu_L|/2 = 1.14$ MHz, close to the 1.12 MHz previously determined from the X-band continuous wave (cw) EPR experiments [17,20] and is in the excellent agreement with $A = -1.15$ MHz determined from the DFT calculations presented in the same references. A small and negative HF coupling with ^{14}N indicates that the spin density distribution is subject of a very specific situation, where the minority spin channel becomes *locally* dominating. While this delicate peculiarity has been theoretically established, the experimental evidence of the HF interaction negative sign, has been remained elusive, since the sign can not be determined by means of cw EPR experiments used in the previous works. For the $m_S = 0$, manifold hyperfine interaction is absent and only quadrupole interaction induces additional splitting of the nuclear spin sublevels manifesting itself in the ENDOR spectra at the frequencies placed symmetrically relative to the ^{14}N Larmor frequency. The corresponding doublets are labeled as $v_{1,3}$ and $v_{5,8}$ on the Figs. 2(b) and 2(c), respectively. Thus, the absolute value of the quadrupole splitting is derived as half of a difference between the frequencies, e.g., v_1 and v_3 , $|P| = 1.81$ MHz.

In order to determine the symmetry of the quadrupole and hyperfine interaction and to justify the collinearity of the all spin Hamiltonian terms, we measured the angular dependence of the ENDOR frequencies for different directions of the magnetic field relative to the symmetry c axis, presented in Fig. 3. All frequencies are described by Eq. (2) with parameters $a = -1.14$ MHz, $b = 0.014$ MHz, and $P = 1.81$ MHz, thus reveal axial anisotropy of the QI and HFI relative to the c axis. The quadrupole-coupling constant for the NV_{kk} in 4H-SiC is determined to be $|C_q| = \frac{4}{3}|P| = 2.44$ MHz. After the symmetry of the QI was determined, it can be concluded that the absolute value of the quadrupole parameter P is equal to $3/2P_z$ and quadrupole interaction tensor components are $P_z = 1.206$ MHz and $P_x = P_y = -0.603$ MHz.

B. Comparison with literature and DFT

In the following, we will discuss the implication of the experimentally observed electron-nuclear interaction onto the microscopic origin of the center. In particular, the quite large quadrupole coupling constant of $|C_q| = 2.44$ MHz provides a characteristic fingerprint.

In literature, values for the quadrupole coupling of ^{14}N nuclei in molecules are typically reported in the range of 1 and 4 MHz (see Refs. [41,42]). Whereas threefold coordinated N (like NH_2 groups) give values between 1 and 2.7 MHz; for larger values up to 4 MHz twofold coordinated nitrogen is required. Fourfold coordinated N, like isolated N donors in SiC, are more or less limited to incorporation in semiconductor matrices. In silicon, in particular in case of ionized donors strain is required to induces nonvanishing coupling constants [43]. Otherwise, the incorporation within T_d symmetry leads to almost isotropic electric field gradients, and by this vanishing quadrupole coupling constants. The situation in the cubic polytype 3C-SiC is similar. Nonzero,

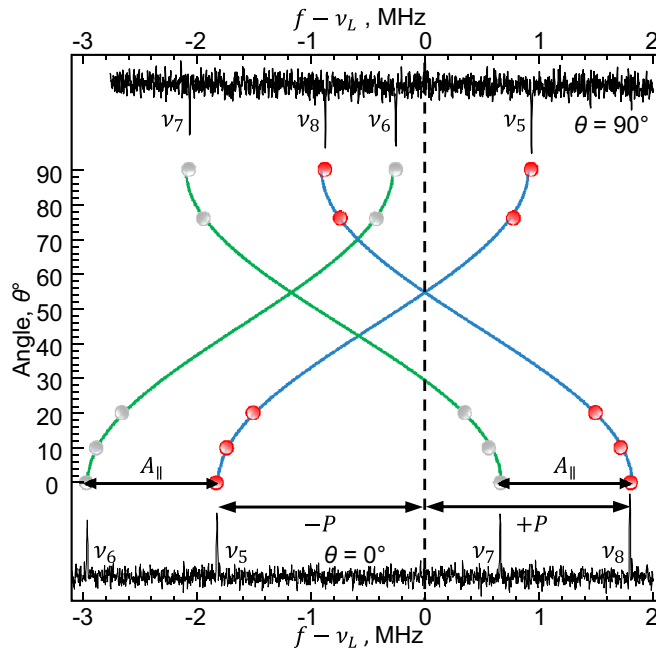


FIG. 3. ENDOR spectra detected in the $(B\parallel c)$ (bottom, $\theta = 0^\circ$) and $B\perp c$ (top, $\theta = 90^\circ$) orientations represented in high-resolution coordinates, i.e., $f - \nu_L$. Measured angular dependence of the ENDOR frequencies is shown in between by red and gray balls together with its fit obtained using Eq. (2) with parameters $a = -1.170$ MHz, $b = 0.014$ MHz, and $P = 1.81$ MHz. Quadrupole splitting parameter P and hyperfine interaction constant (A_{\parallel}) are shown by arrows.

but still quite small quadrupole splittings are observed in the hexagonal polytypes. In $4H$ -SiC, for the ionized N donor at the hexagonal site $(N_C^+)_h$, we calculate $C_q = 0.110$ MHz; for $(N_C^+)_k$ a slightly smaller value of 0.080 MHz is predicted. These values are reflected by the “far” $VV_{kk} + N_C^+$ complexes (see Table I). Less distant configurations show considerable deviations from the ideal values, but with maximum absolute values of +0.41 MHz (N2) and -0.22 MHz (N5) they are still much smaller than the experimentally observed value.

Obviously, the experimentally observed value of $C_q = (-)2.44$ MHz is clearly indicative for a *threefold* coordinated ^{14}N nucleus. Although other, more complicated configurations than the nearest-neighbor pair are in principle possible (like the $V_C V_{Si} N_C$ complex), they are not able to explain the small and nearly isotropic hyperfine interaction. They are furthermore less probable due to symmetry arguments. Only the $N_C V_{Si}^-$ pair is able to explain all the experimentally observed electron-nuclear data simultaneously.

C. Comparison with NV in diamond

After conclusively establishing the microscopic origin of the NV_{kk} centers in $4H$ -SiC, we now further illustrate this assignment by a rational discussion of the spin-interaction parameters in comparison with those of the NV^- center in diamond. By this we will underline the strong similarity between these two centers. Particularly, we would like to stress that the lattice parameter can explain most of the difference in the spectroscopic characteristics between NV centers hosted in the two different crystal matrices, diamond and SiC.

We start from an analysis of the ZFS value. In diamond and overall also in SiC, it is known to be induced by the dipole-dipole interaction between two unpaired electron spins predominantly [28,44]. The positive sign of the D value indicates the oblate distribution of the NVs’ spin density. Thus, ZFS can be expressed in the form $D = \frac{3\mu_0}{16\pi h} (g\mu_B)^2 \frac{1}{\langle r \rangle^3}$. Using this simple approximation and previously established $D = 2.88$ GHz of the NV^- center in diamond [45,46] one can derive the average distance between the unpaired electrons to be $\langle r \rangle \approx 2.4$ Å, comparable to the 2.43 Å—the distance between tetrahedron basal carbon atoms surrounding the carbon vacancy. This intercarbon distance is much larger in SiC and equals to 3.08 Å [see also Fig. 1(a)]. That is one would expect for the SiC NVs’ the ZFS splitting smaller in $3.08^3/2.43^3$ times, i.e., roughly 1.4 GHz. The experimentally obtained $D = 1.288$ GHz nicely reflects this scaling coefficient. The same approach can be applied to the ^{14}N hyperfine interaction and quadrupole coupling constants. In diamond, a small anisotropy can be derived from previously measured values of A_{\parallel} and A_{\perp} as $b = (A_{\parallel} - A_{\perp})/3$, ranging from 0.06 MHz [46,47] up to 0.17 MHz [48,49]. Taking into account the difference of bond lengths in diamond (C-C bond = 1.54 Å) and SiC (Si-C bond = 1.89 Å) one can estimate the dipolar part of the hyperfine interaction in the case of the NV center in SiC to be approximately 30 kHz, not too far from the 14 kHz resolved in our experiments, having in mind the *indirect* character of this hyperfine interaction. Last but not least, the absolute value of the quadrupole coupling constant, established to be in the range of 6.4–6.8 MHz [46–49] for the NV^- center in diamond, is a factor of about 2.6 smaller for the NV_{kk} center in $4H$ -SiC, again roughly reflecting an $\frac{1}{\langle r \rangle^3}$ scaling behavior with respect to the lattice constants.

D. Relaxation times T_2

Both hyperfine and quadrupole interactions are irremovable sources of decoherence for the NV^- centers. Since in SiC they are smaller than in diamond, a longer T_2 time in SiC crystals with low concentration of magnetic moments of any kind is expected.

Recently, Hahn-echo coherence time of the isolated single VV_{kk} divacancy in high purity $4H$ -SiC single crystal with natural isotope content (abundances of ^{29}Si and ^{13}C isotopes, both with $I = 1/2$ are 4, 68% and 1.1%, respectively) has been measured to be $T_2 = 1.3$ ms [50]. This coherence is even longer compared with the Hahn-echo coherence $T_2 = 0.8$ ms measured on the single negatively charged silicon vacancy defect in $4H$ -SiC [51]. That is VV_{kk} seems to possess one of the longest Hahn-echo coherence achieved so far on defects in a naturally isotopic crystal [50]. Here we have used the ability to probe the coherence of spin ensembles of both divacancies and NV centers (in kk configuration) incorporated in the same crystalline matrix. They are thus characterized by the same environment of paramagnetic species and magnetic isotopes (^{29}Si and ^{13}C), i.e., they reside in the same decoherence bath.

We first estimate the limit of the coherence time of VV_{kk} and NV_{kk} spin ensembles if only limitation through homodeficient spin-spin interaction is considered using the following equation $T_2 = \hbar r^3 / 2\pi \mu_B^2$ [52], where r is the distance between the defects of the same type. In the case of NV_{kk} centers

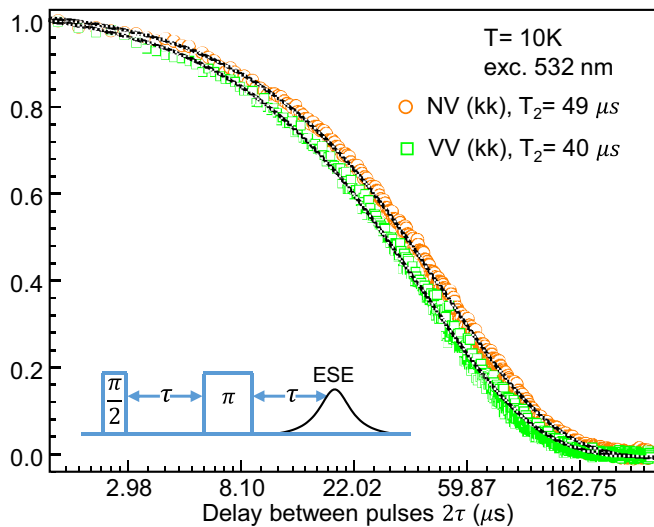


FIG. 4. Coherence times T_2 measured on the ensemble of optically polarized spins of VV_{kk} divacancies (green squares) and NV_{kk} centers (orange circles). Single exponential fit of the experimental relaxation curves (black solid lines) with characteristic decay times $T_2 = 40 \mu\text{s}$ and $T_2 = 49 \mu\text{s}$ for the VV_{kk} and NV_{kk} centers, respectively. Inset illustrates the mw pulse sequence used in the current experiment. Relaxation curve measured on the VV_{hh} centers follows roughly the same exponential decay with $T_2 = 41 \mu\text{s}$ as for the VV_{kk} (not shown for clarity).

the $r \approx \sqrt[3]{1/5 \times 10^{-16} \text{ cm}^3} \approx 27 \text{ nm}$ what corresponds to $T_2 = 241 \mu\text{s}$. For VV_{kk} centers such estimated coherence time is $T_2 = 82 \mu\text{s}$.

Using standard Hahn-echo pulse sequence the T_2 relaxation curves were measured as a function of the time delay τ between mw pulses and are plotted on a logarithmic scale (see Fig. 4). It is seen, though negatively charged NV_{kk} centers in SiC comprises two additional sources of the decoherence (hyperfine and quadrupole interactions) induced by the presence of ^{14}N nuclear spin, its coherence time is comparable with the divacancy centers and even a bit superior (20% larger). A possible reason for this is the electron spin density of the NV center is characterized by slightly higher localization that in the divacancy case, protecting the NVs' electron spin from interactions with remote magnetic moments. The resulting relaxation times of about $50 \mu\text{s}$ look quite promising and are comparable with the T_2 times of the NV^- centers in diamond ranging from a few microseconds [53,54] up to $10 \mu\text{s}$ [55], obtained on the nonoptimized samples. Measured here Hahn-echo coherence of the NV^- spin ensembles is pinned in the range of the silicon vacancy spin ensemble Hahn-echo coherence time since the latter demonstrating the spread from

$4 \mu\text{s}$ up to $130 \mu\text{s}$ depending on the irradiation procedure and crystal type of SiC [56–58].

The measured values of T_2 are significantly shorter than estimates accounting for homo-defect spin-spin interaction exclusively. The latter means, that we probe “diluted” spin ensembles, and their coherence determines mainly by interactions with other paramagnetic species since at the experimental temperature an influence of spin-lattice relaxation is negligibly small.

V. CONCLUSIONS

To summarize, in the present paper we investigated all terms of the NV centers' spin Hamiltonian in $4H$ -SiC by means of high-frequency ($\approx 94 \text{ GHz}$) pulsed EPR spectroscopy. We experimentally determined the sign of the ground state zero-field splitting to be positive. Driving nuclear magnetic resonance transitions associated with ^{14}N nuclear spin ($I = 1$) with RF pulses, we established both the sign of the corresponding hyperfine interaction with the NV-centers' electron spin as well as an absolute value and symmetry of nuclear quadrupole interaction above 2 MHz. The latter is indicative for a threefold coordinated N atom, confirming conclusively the attribution of the observed spectrum to a nearest $\text{N}_\text{C}\text{V}_{\text{Si}}$ - pair. This attribution can be further illustrated: The established terms of the Hamiltonian allowed us to produce comparative analysis of the NV centers in SiC and NV centers in diamond in order to underline the apparent significant similarity of their ground states; almost all parameters of the NV-center in SiC can be obtained by rescaling of the diamonds' NV center parameters by appropriate lattice constants.

In the $4H$ -SiC sample under study, both divacancy centers and NV centers were observed that allowed us to measure and compare the coherence times of the centers found in the identical environmental conditions. The Hahn-echo coherence time measured on the ensemble of the NV_{kk} centers is $T_2 = 49 \mu\text{s}$, slightly longer than that measured for the divacancies ensemble $T_2 = 40 \mu\text{s}$. The latter shows a potential of the NV centers in SiC for applications in quantum technologies.

ACKNOWLEDGMENTS

This work has been supported by the Russian Science Foundation (Project No. 20-72-10068). The DFT calculations have been done using grants of computer time from the Paderborn Center for Parallel Computing (PC²) and have been also supported by the DFG priority program SPP 1601.

- [1] L. Childress, R. Walsworth, and M. Lukin, Atom-like crystal defects: From quantum computers to biological sensors, *Phys. Today* **67**(10), 38 (2014).
 [2] D. Awschalom, R. Hanson, J. Wrachtrup, and B. B. Zhou, Quantum technologies with optically interfaced solid-state spins, *Nat. Photon.* **12**, 516 (2018).

- [3] M. Atatüre, D. Englund, N. Vamivakas, S.-Y. Lee, and J. Wrachtrup, Material platforms for spin-based photonic quantum technologies, *Nat. Rev. Mater.* **3**, 38 (2018).
 [4] A. Gottscholl, M. Kianinia, V. Soltamov, S. Orlinskii, G. Mamin, C. Bradac, C. Kasper, K. Krambrock, A. Sperlich, M. Toth, I. Aharonovich, and V. Dyakonov, Initialization and

- read-out of intrinsic spin defects in a van der Waals crystal at room temperature, *Nat. Mater.* **19**, 540 (2020).
- [5] M. W. Doherty, N. B. Manson, P. Delaney, F. Jelezko, J. Wrachtrup, and L. C. L. Hollenberg, The nitrogen-vacancy colour centre in diamond, *Phys. Rep.* **528**, 1 (2013).
- [6] P. C. Humphreys, N. Kalb, J. P. J. Morits, R. N. Schouten, R. F. L. Vermeulen, D. J. Twitchen, M. Markham, and R. Hanson, Deterministic delivery of remote entanglement on a quantum network, *Nature (London)* **558**, 268 (2018).
- [7] C. L. Degen, F. Reinhard, and P. Cappellaro, The nitrogen-vacancy colour centre in diamond, *Rev. Mod. Phys.* **89**, 035002 (2017).
- [8] H. Zheng, J. Xu, G. Z. Iwata, T. Lenz, J. Michl, B. Yavkin, K. Nakamura, H. Sumiya, T. Ohshima, J. Isoya, J. Wrachtrup, A. Wickenbrock, and D. Budker, Zero-Field Magnetometry Based on Nitrogen-Vacancy Ensembles in Diamond, *Phys. Rev. Appl.* **11**, 064068 (2019).
- [9] J. D. Breeze, E. Salvadori, J. Sathian, N. McN. Alford, and Ch. W. M. Kay, Continuous-wave room-temperature diamond maser, *Nature (London)* **555**, 493 (2018).
- [10] J. R. Weber, W. F. Koehl, J. B. Varley, A. Janotti, B. B. Buckley, C. G. Van de Walle, and D. D. Awschalom, Quantum computing with defects, *Proc. Natl. Acad. Sci. USA* **107**, 8513 (2010).
- [11] P. G. Baranov, A. P. Bundakova, A. A. Soltamova, S. B. Orlinskii, I. V. Borovykh, R. Zondervan, R. Verberk, and J. Schmidt, Silicon vacancy in SiC as a promising quantum system for single-defect and single-photon spectroscopy, *Phys. Rev. B* **83**, 125203 (2011).
- [12] W. F. Koehl, B. B. Buckley, F. J. Heremans, G. Calusine, and D. D. Awschalom, Room temperature coherent control of defect spin qubits in silicon carbide, *Nature (London)* **479**, 84 (2011).
- [13] G. V. Astakhov, D. Simin, V. Dyakonov, B. V. Yavkin, S. B. Orlinskii, I. I. Proskuryakov, A. N. Anisimov, V. A. Soltamov, and P. G. Baranov, Spin centres in SiC for quantum technologies, *Appl. Magn. Reson.* **47**, 793 (2016).
- [14] S. A. Tarasenko, A. V. Poshakinskiy, D. Simin, V. A. Soltamov, E. N. Mokhov, P. G. Baranov, V. Dyakonov, and G. V. Astakhov, Spin and optical properties of silicon vacancies in silicon carbide—A review, *Phys. Status Solidi B* **255**, 1700258 (2018).
- [15] A. L. Falk, B. B. Buckley, G. Calusine, W. F. Koehl, V. V. Dobrovitski, A. Politi, C. A. Zorman, P. X.-L. Feng, and D. D. Awschalom, Polytype control of spin qubits in silicon carbide, *Nat. Commun.* **4**, 1819 (2013).
- [16] H. J. von Bardeleben, J. L. Cantin, E. Rauls, and U. Gerstmann, Identification and magneto-optical properties of the NV center in 4H-SiC, *Phys. Rev. B* **92**, 064104 (2015).
- [17] H. J. von Bardeleben, J. L. Cantin, A. Csore, A. Gali, E. Rauls, and U. Gerstmann, NV centers in 3C, 4H, and 6H silicon carbide: A variable platform for solid-state qubits and nanosensors, *Phys. Rev. B* **94**, 121202(R) (2016).
- [18] S. A. Zargaleh, H. J. von Bardeleben, J. L. Cantin, U. Gerstmann, S. Hameau, B. Eblé, and Weibo Gao, Electron paramagnetic resonance tagged high-resolution excitation spectroscopy of NV-centers in 4H-SiC, *Phys. Rev. B* **98**, 214113 (2018).
- [19] U. Gerstmann, E. Rauls, Th. Frauenheim, and H. Overhof, Formation and annealing of nitrogen-related complexes in SiC, *Phys. Rev. B* **67**, 205202 (2003).
- [20] Z. Mu, S. A. Zargaleh, H. J. von Bardeleben, J. E. Fröch, M. Nonahal, H. Cai, X. Yang, J. Yang, X. Li, I. Aharonovich, and W. Gao, Coherent manipulation with resonant excitation and single emitter creation of nitrogen vacancy centers in 4H silicon carbide, *Nano Lett.* **20**, 6142 (2020).
- [21] D. J. Christle, P. V. Klimov, C. F. de las Casas, K. Szász, V. Ivády, V. Jokubavicius, J. Hassan, M. Syväjärvi, W. F. Koehl, T. Ohshima, N. T. Son, E. Janzén, A. Gali, and D. D. Awschalom, Isolated Spin Qubits in SiC with a High-Fidelity Infrared Spin-to-Photon Interface, *Phys. Rev. X* **7**, 021046 (2017).
- [22] A. Lohrmann, B. C. Johnson, J. C. McCallum, and S. Castelletto, A review on single photon sources in silicon carbide, *Rep. Prog. Phys.* **80**, 034502 (2017).
- [23] V. S. Vainer and V. A. Il'in, Electron spin resonance of exchange-coupled vacancy pairs in hexagonal silicon carbide, *Sov. Phys. Solid State* **23**, 2126 (1981).
- [24] P. G. Baranov, I. V. Il'in, E. N. Mokhov, M. V. Muzafarova, S. B. Orlinskii, and J. Schmidt, EPR identification of the triplet ground state and photoinduced population inversion for a Si-C divacancy in silicon carbide, *JETP Lett.* **82**, 441 (2005).
- [25] J. Isoya, T. Umeda, N. Mizuochi, N. T. Son, E. Janzén, and T. Ohshima, EPR identification of intrinsic defects in SiC, *Phys. Status Solidi B* **245**, 1298 (2008).
- [26] W. E. Carlos, N. Y. Garces, and E. R. Glaser, Annealing of multivacancy defects in 4H-SiC, *Phys. Rev. B* **74**, 235201 (2006).
- [27] J. P. Perdew, K. Burke, and M. Ernzerhof, Generalized Gradient Approximation Made Simple, *Phys. Rev. Lett.* **78**, 1396 (1997).
- [28] T. Biktagirov, W. G. Schmidt, and U. Gerstmann, Spin decontamination for magnetic dipolar coupling calculations: Application to high-spin molecules and solid-state spin qubits, *Phys. Rev. Res.* **2**, 022024(R) (2020).
- [29] H. J. von Bardeleben, J. L. Cantin, H. Vrielinck, F. Callens, L. Binet, E. Rauls, and U. Gerstmann, Nitrogen split interstitial center (N-N)N in GaN: High frequency EPR and ENDOR study, *Phys. Rev. B* **90**, 085203 (2014).
- [30] Ch. J. Pickard and F. Mauri, First-Principles Theory of the EPR g Tensor in Solids: Defects in Quartz, *Phys. Rev. Lett.* **88**, 086403 (2002).
- [31] P. Giannozzi *et al.*, QUANTUM ESPRESSO: A modular and open-source software project for quantum simulations of materials, *J. Phys.: Condens. Matter* **21**, 395502 (2009).
- [32] P. Giannozzi *et al.*, Advanced capabilities for materials modelling with Quantum ESPRESSO, *J. Phys.: Condens. Matter* **29**, 465901 (2017).
- [33] U. Gerstmann, Ab initio Green's function calculation of hyperfine interactions for shallow defects in semiconductors, *Phys. Status Solidi B* **248**, 1319 (2011).
- [34] P. E. Blöchl, First-principles calculations of defects in oxygen-deficient silica exposed to hydrogen, *Phys. Rev. B* **62**, 6158 (2000).
- [35] A. Csóré, H. J. Von Bardeleben, J. L. Cantin, and A. Gali, Characterization and formation of NV centers in 3C, 4H, and 6H SiC: An ab initio study, *Phys. Rev. B* **96**, 085204 (2017).
- [36] S. Stoll and A. Schweiger, EasySpin, A comprehensive software package for spectral simulation and analysis in EPR, *J. Magn. Reson.* **178**, 42 (2006).
- [37] See Supplemental Material at <http://link.aps.org/supplemental/10.1103/PhysRevB.103.245203> for more information about the estimation of the divacancies concentration in the sample.

- [38] W. B. Mims, Pulsed ENDOR experiments, Proc. R. Soc. London, Ser. A **283**, 452 (2006).
- [39] Bruker: Almanac 2011, Bruker Biospin, Rheinstetten (2011), p. 47.
- [40] J.-M. Spaeth, J. R. Niklas, and R. H. Bartram, in *Structural Analysis of Point Defects in Solids* (Springer-Verlag, Berlin, Heidelberg, 1992), Chap. 5, p. 152.
- [41] S. Stoll and D. Goldfarb, EPR interactions–Nuclear quadrupole couplings, *eMagRes* **6**, 495 (2017).
- [42] F. MacMillan, S. Kacprzak, P. Hellwig, S. Grimaldi, H. Michel, and M. Kaupp, Ilucidating mechanisms in haem copper oxidases: The high-affinity QH binding site in quinol oxidase as studied by DONUT-HYSCORE spectroscopy and density functional theory, *Faraday Discuss.* **148**, 315 (2011).
- [43] D. P. Franke, F. M. Hrubesch, M. Künzl, H.-W. Becker, K. M. Itoh, M. Stutzmann, F. Hoehne, L. Dreher, and M. S. Brandt, Interaction of Strain and Nuclear Spins in Silicon: Quadrupolar Effects on Ionized Donors, *Phys. Rev. Lett.* **115**, 057601 (2015).
- [44] T. Biktagirov and U. Gerstmann, Spin-orbit driven electrical manipulation of the zero-field splitting in high-spin centers in solids, *Phys. Rev. Res.* **2**, 023071 (2020).
- [45] J. H. N. Loubser and J. A. van Wyk, Electron spin resonance in the study of diamond, *Rep. Prog. Phys.* **41**, 1201 (1978).
- [46] X. F. He, N. B. Manson, and P. T. H. Fisk, Paramagnetic resonance of photoexcited N-V defects in diamond. II Hyperfine interaction with the ^{14}N nucleus, *Phys. Rev. B* **47**, 8809 (1993).
- [47] C. S. Shin, M. C. Butler, H.-J. Wang, C. E. Avalos, S. J. Seltzer, R.-B. Liu, A. Pines, and V. S. Bajaj, Optically detected nuclear quadrupolar interaction of N in nitrogen-vacancy centers in diamond, *Phys. Rev. B* **89**, 205202 (2014).
- [48] S. Felton, A. M. Edmonds, M. E. Newton, P. M. Martineau, D. Fisher, D. J. Twitchen, and J. M. Baker, Hyperfine interaction in the ground state of the negatively charged nitrogen vacancy center in diamond, *Phys. Rev. B* **79**, 075203 (2009).
- [49] B. V. Yavkin, G. V. Mamin, and S. B. Orlinskii, High-frequency pulsed ENDOR spectroscopy of the NV centre in the commercial HPHT diamond, *J. Magn. Reson.* **262**, 15 (2016).
- [50] H. Seo *et al.*, Quantum decoherence dynamics of divacancy spins in silicon carbide, *Nat. Commun.* **7**, 12935 (2016).
- [51] R. Nagy, M. Niethammer, M. Widmann, Y.-C. Chen, P. Udvarhelyi, C. Bonato, J. Ul Hassan, R. Karhu, I. G. Ivanov, N. T. Son, J. R. Maze, T. Ohshima, Ö. O. Soykal, Á. Gali, S.-Y. Lee, F. Kaiser, and J. Wrachtrup, High-fidelity spin and optical control of single silicon-vacancy centres in silicon carbide, *Nat. Commun.* **10**, 1954 (2019).
- [52] *Distance Measurements in Biological Systems by EPR*, edited by L. J. Berliner, S. S. Eaton, G. R. Eaton (Springer Science Business Media, New York, NY, 2006), Vol. 19.
- [53] F. T. Charnock and T. A. Kennedy, Combined optical and microwave approach for performing quantum spin operations on the nitrogen-vacancy center in diamond, *Phys. Rev. B* **64**, 041201(R) (2001).
- [54] B. V. Yavkin, G. V. Mamin, S. B. Orlinskii, S. V. Kidalov, F. M. Shakhov, A. Ya. Vul', A. A. Soltamova, V. A. Soltamov, and P. G. Baranov, Room temperature high-field spin dynamics of nv defects in sintered diamonds, *Appl. Magn. Reson.* **44**, 1235 (2013).
- [55] S. Takahashi, R. Hanson, J. van Tol, M. S. Sherwin, and D. D. Awschalom, Quenching Spin Decoherence in Diamond through Spin Bath Polarization, *Phys. Rev. Lett.* **101**, 047601 (2008).
- [56] P. G. Brereton, D. Puent, J. Vanhoy, E. R. Glaser, and S. G. Carter, Spin coherence as a function of depth for high-density ensembles of silicon vacancies in proton-irradiated 4H-SiC, *Solid State Commun.* **320**, 114014 (2020).
- [57] D. Simin, H. Kraus, A. Sperlich, Ohshima, G. V. Astakhov, and V. Dyakonov, Locking of electron spin coherence above 20 ms in natural silicon carbide, *Phys. Rev. B* **95**, 161201(R) (2017).
- [58] C. Kasper, D. Klenkert, Z. Shang, D. Simin, A. Gottscholl, A. Sperlich, H. Kraus, C. Schneider, S. Zhou, M. Trupke, W. Kada, T. Ohshima, V. Dyakonov, and G. V. Astakhov, Influence of Irradiation on Defect Spin Coherence in Silicon Carbide, *Phys. Rev. Appl.* **13**, 044054 (2020).